Annu. Rev. Biophys. Biomol. Struct. 1994. 23:1–25

FIELD GRADIENT ESR AND MOLECULAR DIFFUSION IN MODEL MEMBRANES

J. H. Freed

Baker Laboratory of Chemistry, Cornell University,
Ithaca, New York 14853

KEY WORDS: phospholipids, cholesterol, order parameters, free volume model, spectral-spatial imaging

CONTENTS

INTRODUCTION

The dynamic behavior of biomembranes occupies a central focus of modern membrane research (26). In particular, translational diffusion of lipids and proteins is essential for various biological processes (26). The techniques developed to measure the translational diffusion coefficients in model or biomembranes can be divided into two general categories according to their relevant distance scales. Modern macroscopic methods include NMR-spin echo (8, 39), fluorescence recov-

1056-8700/94/0610-0001$05.00

ery after photobleaching (FRAP) (59, 74) and dynamic imaging of diffusion by electron spin resonance (ESR) (5, 47, 65, 68, 70). These enable one to study how the bulk distribution of labeled molecules changes with time and they have resolution on the order of a few to several hundred micrometers. Microscopic methods allow one to observe diffusion over the order of molecular diameters, i.e. a few tens of Ångstroms. Such techniques typically reveal diffusion via encounters between labeled molecules through excimer formation (49), quasi-elastic neutron scattering (55), NMR T_1 relaxation measurements (75), or Heisenberg spin exchange (4, 15, 50, 56, 60, 72).

Macroscopic experiments are usually interpreted in terms of simple phenomenological descriptions of diffusion (e.g. Fick's law) to yield the diffusion coefficient. The pulsed field-gradient NMR technique has been utilized to study diffusional processes in model membranes and related systems (38, 39, 51, 75). Although this method can measure the self-diffusion coefficient of the actual solvent molecules, it is limited by the short T_2 for membranes ($\sim$10 μs to $\sim$1 ms). To measure even fairly large diffusion coefficients, i.e. $D \approx 10^{-7}$ to $\sim 10^{-5}$ cm^2 s^{-1}, one needs at least several Teslas cm^{-1} field gradients (51). FRAP is by far the most commonly used technique to measure the lateral diffusion coefficient for lipids in membranes (59, 74) and enables the investigator to measure a wide range of diffusion coefficients (10^{-12} to 10^{-6} cm^2 s^{-1}). Despite the widespread applicability of the FRAP technique to the study of diffusion of macromolecular additives such as proteins and polypeptides, there is an intrinsic problem in using the technique for the study of diffusion of the basic components in mixed membranes such as phospholipids and cholesterol. The size of the photosensitive functional group attached to the parent molecules is usually quite substantial, allowing it to dominate the diffusional process; this can mask the subtle dynamic properties of the individual components (1, 27). More recently the technique of dynamic imaging of diffusion (DID)-ESR was introduced and applied to the study of lateral diffusion of spin-labeled molecules in lipid membranes. In general, one may use nitroxide spin-labeled lipids, cholesterol, peptides, and/or proteins. The nitroxyl functional group is relatively small and therefore will not introduce a large perturbation in most cases. This method and its recent applications are the principle subject of this review.

For microscopic methods, unlike macroscopic methods, the analysis leading to the relative diffusion coefficient depends heavily upon the choice of the microscopic molecular dynamic model; this stricture can result in considerable uncertainty in the estimated diffusion coefficient. Also, because such methods detect encounters between labeled mol-

ecules, how the labeled molecule mixes in the fluid is relevant. In magnetic resonance a further difficulty can arise from the complexity of interpreting the spin relaxation (4, 50, 75). Nevertheless, these methods are extremely important for investigating the microscopic dynamic molecular structure of membranes. Several groups have used microscopic ESR methods to measure translational diffusion over distances of molecular dimensions in model membranes (4, 22, 56, 60). Although ESR techniques can potentially be used to study the diffusion of components at a microscopic scale in mixed membranes, there have been no reports on this matter. The limits and drawbacks of the various macroscopic and microscopic methods necessitates the development of new techniques that are reliable and can accurately determine the diffusion coefficient in membranes.

ESR is very useful in the study of dynamic properties of membrane components (36) because of its high sensitivity and favorable time scale. In particular, the DID-ESR imaging method developed in thesc laboratories can be employed to accurately and conveniently measure macroscopic diffusion coefficients of spin probes in model membranes (68, 70). Moreover, the usual ESR spectra can be analyzed with ESR spectral simulation to simultaneously obtain orientational order parameters and rotational diffusion rates. Such a combined study can provide better insight into the dynamical properties of membranes (65, 69, 70).

The first experiments that used ESR imaging to measure diffusion coefficients (3, 9–11, 25, 32, 33) either required long experimental times (e.g. 10 days) (33) or assumed an idealized model for the analysis (9). However, developments such as the use of Fourier-space analysis of the data (5, 46, 47), along with narrow initial spin probe concentration profiles, reduced the experimental time by about four orders of magnitude (e.g. to 1 h for $D \approx 10^{-8}$ cm^2 s^{-1}), yet allowed a high degree of accuracy in studies of lateral diffusion in model membranes.

The DID-ESR method is based upon continuous wave (cw)-ESR experiments in the presence of field gradients to achieve spatial resolution (16). In principle, one can apply ESR experiments analogous to pulsed field-gradient NMR to measure diffusion. Unfortunately, because the ESR time scale is so much faster than that of NMR, the pulsed field gradient method cannot be applied to diffusion coefficients for which D is less than about 10^{-1} cm^2 s^{-1}. However, in fluids including membranes the molecules exhibit $D < 10^{-5}$ cm^2 s^{-1}. The cw-DID-ESR method is capable of measuring the latter values. Nevertheless, modern pulse and Fourier transform ESR methods do have their place in the study of molecular diffusion, as recent developments have indicated.

THE DID-ESR METHOD

The measurement of the diffusion coefficient, D, by DID-ESR involves two stages. After preparing the sample with an inhomogeneous distribution of spin probes along a given direction, the investigator uses the ESR imaging method to obtain the (one-dimensional) concentration profiles at several different times. Spatial resolution results from the magnetic field gradient, because spin probes at each spatial point experience a different resonant frequency. With time, this inhomogeneous distribution will move toward a homogeneous distribution via translational diffusion. The second stage is to fit the time-dependent concentration profiles to the diffusion equation in order to obtain D.

The ESR spectrum recorded in the presence of a magnetic field gradient B' (G cm^{-1}) is a convolution of the usual ESR spectrum (gradient-off spectrum), $I_o(\xi)$, with the concentration of spin probes $C(x,t)$ (33):

$$I_g(\xi,t) = \int_{-\infty}^{\infty} C(\xi',t)I_o(\xi - \xi')\, d\xi', \qquad 1.$$

where $\xi \equiv (B - B_o)$ measures the spectral position as the deviation of the magnetic field B from the field B_o at the nominal center of the spectrum, corresponding to the position $x = 0$, since B' maps x onto $\xi = B'x$. Thus the variable ξ is used in place of x and B in the development below. The concentration of spin probe at any position in the sample is kept low enough that the spectral shape does not vary from position to position owing to Heisenberg spin exchange.

The determination of $C(\xi,t)$ from the two spectra $I_g(\xi,t)$ and $I_o(\xi)$ is, in principle, a straightforward calculation. If the Fourier transform of the two spectra are represented as

$$\hat{I}_g(\kappa,t) = \int_{-\infty}^{\infty} I_g(\xi,t) \exp(-2\pi i\kappa\xi)\, d\xi \qquad 2a.$$

$$\hat{I}_o(\kappa) = \int_{-\infty}^{\infty} I_o(\xi) \exp(-2\pi i\kappa\xi)\, d\xi, \qquad 2b.$$

where κ is the inverse wavelength associated with ξ, then the Fourier transform of both sides of Equation 1 yields

$$\hat{I}_g(\kappa,t) = \hat{C}(\kappa,t)\hat{I}_o(\kappa), \qquad 3.$$

where $\hat{C}(\kappa,t)$ is the Fourier transform of $C(\xi,t)$. Therefore $C(\xi,t)$ is equal to

$$C(\xi,t) = \int_{-\infty}^{\infty} [\hat{I}_g(\kappa,t)/\hat{I}_o(\kappa)]W(\kappa) \exp(2\pi i\kappa\xi)\, d\kappa, \qquad 4.$$

where we have inserted $W(\kappa)$, a filter function necessary for the indicated division. An analysis that depends on $C(\xi,t)$ in real space will suffer from the accumulated errors of two forward Fourier transformations, one filtered division, and one back Fourier transformation (33). One can avoid the back transform step and the use of a filter function by analyzing the data in Fourier space. Also, only those Fourier components with sufficient sensitivity to the diffusion need be included, as noted below.

The usual one-dimensional diffusion equation is written in terms of the universal variable ξ as (7):

$$\frac{\partial C(\xi,t)}{\partial t} = D_\xi \frac{\partial^2 C(\xi,t)}{\partial \xi^2}, \qquad 5.$$

where $D_\xi \equiv D(B'^2)$ (i.e. the units of D_ξ are $G^2\ s^{-1}$). The ideal experiment would be the diffusion of spin probes from an instantaneous point source (δ-function). If the source is placed at $x = 0$ at $t = 0$, then the solution of Equation 5 is $C(\xi,t) = [C_o/(4\pi D_\xi t)^{1/2}] \exp[-(\xi^2/4D\xi t)]$, which is a Gaussian concentration profile for all time. For an arbitrary initial distribution of spin probes, in the absence of boundary effects, the solution is a convolution of the initial distribution $C(\xi,t = 0)$ with the solution for the point source:

$$C(\xi,t) = [1/(4\pi D_\xi t)^{1/2}] \int_{-\infty}^{\infty} \exp[-(\xi - \xi')^2/4D_\xi t] C(\xi,t = 0)\, d\xi'. \qquad 6.$$

Taking the Fourier transform of both sides, one obtains $\hat{C}(\kappa,t) = \exp(-4\pi^2\kappa^2 D_\xi t)\hat{C}(\kappa,0)$ or alternatively,

$$\ln \hat{C}(\kappa,t) - \ln \hat{C}(\kappa,0) = -4\pi^2 D_\xi \kappa^2 t. \qquad 7.$$

Only the amplitude of $\hat{C}(\kappa,t)$ changes as a function of time as a result of the diffusion process (5, 46). Note that $\hat{C}(\kappa,t)$ is obtained from Equation 3.

If the initial spin probe distribution is well approximated by a Gaussian (68), then

$$C(\xi) = \frac{C_0}{\sqrt{2\pi}\,\delta_\xi} \exp\left[-\left(\frac{\xi^2}{2\delta_\xi^2}\right)\right], \qquad 8.$$

where δ_ξ is the variance and C_0 is a measure of the maximum value of $C(\xi)$. Very narrow initial distributions, even of irregular shape, quickly develop into a Gaussian because of diffusion (46). One can start the experiment at such a time; then Equations 7 and 8 apply, yielding

$\ln |\hat{C}(\kappa,t)| = -2\pi^2\sigma_\xi^2(t)\kappa^2 + \ln C_o$, where $\sigma_\xi^2(t) = \delta_\xi^2 + 2D_\xi t$. Thus, by plotting $\hat{C}(\kappa,t)$, with respect to κ^2 one obtains the slope $-2\pi^2\sigma_\xi^2(t)$. Then a plot of $\sigma_\xi^2(t)$ with respect to t yields $D = D_\xi B'^{-2}$ from the slope. Graphs of $\ln \hat{C}(\kappa,t)$ vs κ^2 for CSL spin probe in a POPC (see Table 1, below, for full names) model membrane were linear up to a maximum in κ^2, showing the concentration profile is well approximated by a Gaussian (5).

The diffusion constants of CSL in the POPC model membrane (5) at various temperatures derived from the ESR imaging technique are close in value to those of fluorescence probes as measured by FRAP (74). The small difference that was observed may result from the structural differences of the probe molecules used in those two techniques.

For samples that do not have a Gaussian spin probe distribution, one can perform the analysis by pairing the profiles at different times (5). Given two concentration profiles obtained at different times, t_i and t_j, Equations 3 and 7 shows that a plot of $\ln |I_g(\kappa,t_j)| - \ln |\hat{I}_g(\kappa,t_i)|$ vs $\kappa^2\Delta(t_i - t_j)$ yields a slope equal to $-4\pi^2 D_\xi$.

A practical consideration arises in locating the range of κ modes that provide accurate data on the diffusion coefficient. Whereas the high (or low) κ modes are the most (or least) sensitive to D, the κ^2 dependence in Equation 7 causes the modes' amplitudes to be low (or high). Thus, there is an optimum range of κ modes (see 46 for a useful procedure to locate this range). The accompanying analysis has led to the inequality $D_x t_D > (\Delta_B^2/B'^2 + \delta_\xi^2)\epsilon_\kappa^{-1}(1 + 1/\ln \epsilon_\kappa)$, where Δ_B^2 is the variance of the EPR line [i.e. the root mean square (rms) width of a Gaussian EPR line in the absence of a field gradient], ϵ_κ is the signal-to-noise ratio in the Fourier domain (assumed to obey $\epsilon_\kappa \gg 2.4$), and δ_ξ^2 is the variance of (a Gaussian) concentration profile at the beginning of the measurement. This expression sets the lower limit on the diffusion coefficient that can be estimated in a given time, t_D. For example, Shin et al (65) report an ϵ_κ of the order of 50. One can prepare dynamic model membrane samples or liquid crystal samples that have an initial spin probe distribution as narrow as $\delta_x = 2$ mm. The usual ESR line width varies from $2\Delta_B = 0.5$ G to 2 G. Therefore, for a 1-h measurement ($t_D = 4000$ s) with a 100 G cm^{-1} field gradient, one can measure a diffusion coefficient as slow as 2–4 $\times 10^{-9}$ cm^2 s^{-1}.

One can also estimate the optimum gradient (46, 47). For example, under operating conditions of $\epsilon_\kappa = 50$, $t_D = 4000$ s, $D_x = 10^{-8}$ cm^2 s^{-1}, and $\delta_x^2 = 0.01$ cm^2, the optimum B'^2 approximately equals 40 cm^{-2} $\times \Delta_B^2$, which is in fairly good agreement with the gradients used in practice (80–100 G cm^{-1}).

Pali et al (52) recently described a variation of this technique. Instead

of preparing samples with a thin strip containing labeled molecules, they produce a negative (i.e. a sample with a substantial uniform concentration of spins, except in a small strip). They also used a time-modulated magnetic-field gradient, which permits direct observation of spatial distributions without numerical Fourier transformation.

DID-ESR STUDIES ON MIXED MODEL MEMBRANES AND RELATED STUDIES

Lateral Diffusion of Cholesterol and Lipid

The applicability of DID-ESR to measurement of the lateral diffusion coefficient, D, in model membrane has been demonstrated by us in investigations of the effects of cholesterol on the dynamics of two different spin probes, the sterol type CSL (cf Table 1) and the phospholipid type 16-PC (cf Table 1) in phospholipid-cholesterol oriented multilayer model membranes (46, 68, 70). Furthermore, an analysis using EPR spectral simulation methods of the gradient-off spectra collected in the course of the DID-ESR experiment determined the order parameter, S, and the rotational diffusion coefficient, $R_\perp$, for the same sample (24, 62). The choice of spin probes that mimicked either cholesterol (CSL) or phospholipid (16-PC) behavior enabled in-depth considerations of the effects of the membrane composition and temperature on the dynamic molecular structure of the membranes.

Figure 1 shows results on D vs the cholesterol mole fraction, x, over a temperature range of 15–60°C for a binary lipid–cholesterol system. Quite different dependences of D_{CSL} and $D_{\text{16-PC}}$ upon x are evident. The presence of cholesterol influences the cholesterol diffusion more

Table 1 Fits of lateral diffusion coefficient to an activation energy dependent upon S[a]

System[b,c]	D° ($cm^2\ s^{-1}$)	a'[d] (K)	b'[d] (K^2)	β (K)
CSL in POPC/cholesterol[e]	9.18×10^{-6}	−3364	1.30×10^{6}	1303
CSL in DMPC/POPC/cholesterol	1.16×10^{-7}	−4363	1.55×10^{6}	~0
16-PC in POPC/cholesterol	1.06×10^{-4}	-2.60×10^{4}	8.56×10^{6}	2317

[a] From Ref. 68. See Equations 9 and 10.

[b] CSL, 3-doxyl derivative of cholestane-3-one; 16-PC, 1-palmitoyl-2-(16doxyl stearoyl) phosphatidylcholine; POPC, 1-palmitoyl-2-oleoyl-*sn*-glycero-phosphatidylcholine; DMPC, 1,2-dimyristoyl-*sn*-glycero-phosphatidylcholine.

[c] 17 wt% H_2O.

[d] $\alpha(T)$ of Equation 10 is given by $\alpha(T) = a' + b'/T$.

[e] A reanalysis of these data shows that $\alpha(T)$ fits better to the quadratic function $(-18.1 \times 10^3) + (1.07 \times 10^7/T) - (1.48 \times 10^9/T^2)$. The graph in Figure 3 is unaffected, since it utilized the experimental values of $\alpha(T)$ (cf 68).

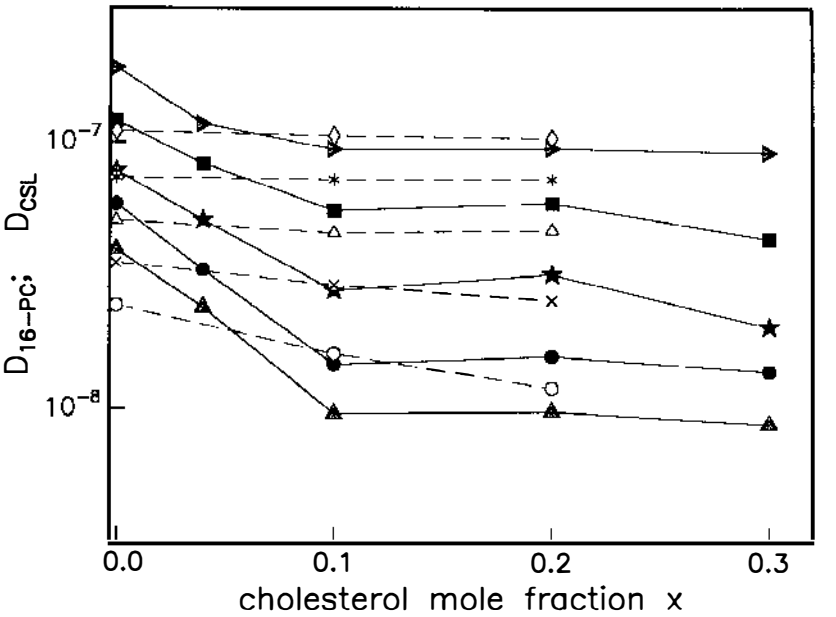

Figure 1 Plots of the variation of D_{CSL} *(solid lines)* and $D_{16\text{-}PC}$ *(dashed lines)* with cholesterol mole fraction x at different temperatures in POPC-cholesterol mixtures. Temperatures: for CSL 15 *(shaded triangles)*, 25 *(shaded circles)*, 35 *(shaded stars)*, 48 *(solid squares)*, and 60°C *(shaded arrowheads)*; for 16-PC 15 *(open circles)*, 24 (×), 35 *(open triangles)*, 48 *(asterisks)*, and 60°C *(open diamonds)*. Data from Ref. 68.

than that of the phospholipid. Also, the observed nonlinear variations of the diffusion coefficients are characteristic of a nonideal solution, because in an ideal solution, the self-diffusion rate should be linear with composition (31). Related nonlinear variations (described below) appear in the order parameter, S (cf Figure 2), and in the rotational diffusion coefficient, $R_\perp$ obtained from the ESR spectral simulations. These studies showed a preferential association of cholesterol molecules with each other in the lipid solvent. In dilute solution, this tendency of the cholesterol (including CSL) molecules to aggregate means that the environment of CSL changes significantly as a function of x, from that of flexible lipid molecules to the more rigid cholesterol molecules. A cholesterol rich region would be more dense and compact than the pure lipid bilayer, thus providing less room for the molecules to diffuse. As a result, the self-diffusion of CSL in such a region should be slower than in the pure lipid bilayer. The tendency of cholesterol to aggregate means that the lipid-rich regions are less influenced by cholesterol molecules than would otherwise be expected. This obser-

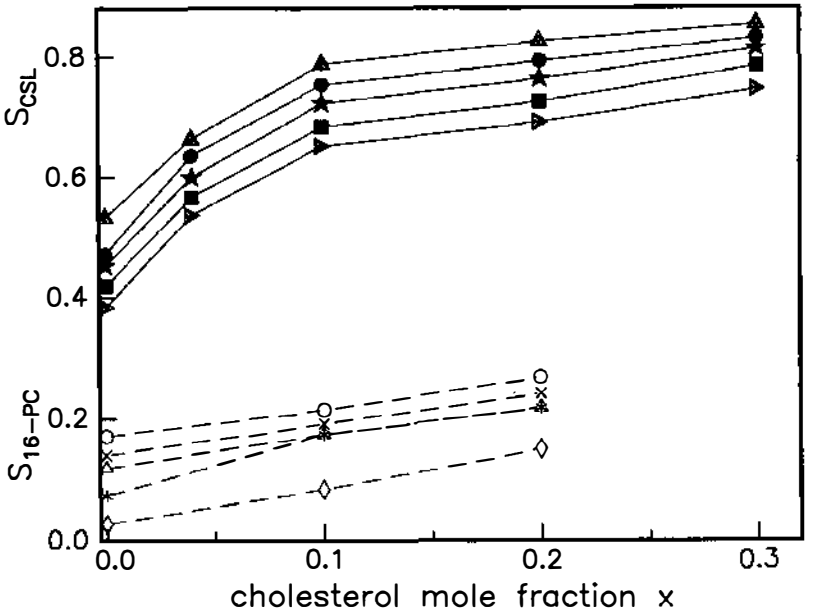

Figure 2 Plots of the $S(x,T)$ for CSL and for 16-PC vs cholesterol mole fraction x at different temperatures in POPC-cholesterol mixtures. See Figure 1 for labeling of points. Data from Ref. 68.

vation is consistent with the rather modest effect of cholesterol on the lateral diffusion of 16-PC.

Self-association, creating larger and more cholesterol-rich regions or clusters, possibly competes with the creation of new clusters in the nonideal solution. The observed saturation effect on D_{CSL} for $x > 0.1$ (cf Figure 1) suggests that the addition of more cholesterol merely increases the extent, but not the nature, of the cholesterol-rich clusters. This may be thought of as a preseparation regime of the nonideal solution. Experiments with CSL in DMPC-POPC-cholesterol ternary mixtures (cf Table 1) show a weaker effect of cholesterol on D_{CSL}, indicating that addition of the saturated lipid DMPC to the unsaturated lipid POPC enhances the mixing of cholesterol in phosphatidylcholine model membranes (70).

In general, the deviations of the D_{CSL} and $D_{16\text{-}PC}$ temperature dependences from Arrhenius behavior at each composition suggest a temperature-dependent activation energy. However, for large x (>0.3) and low temperatures (≤32°C), D_{CSL} for the DMPC-POPC-cholesterol system remained constant with the temperature. This constancy was at-

tributed to a phase separation (70) that occurs at high cholesterol concentration (40, 64, 69).

Comparison with Other Techniques

Previous studies of lateral diffusion by other techniques (1, 27, 39, 42, 59, 78) have almost all focused upon phospholipid diffusion. The DID-ESR results for $D_{16\text{-PC}}$ do not exhibit significant cholesterol influence. A pulsed NMR study of the same system (42) also showed little effect of the cholesterol on the self-diffusion of the POPC molecules. Only FRAP studies of lateral diffusion in DMPC and egg-PC model membranes containing cholesterol (1, 27) investigated both fluorescence-labeled sterol and phospholipid. However, the results of these experiments significantly differed from the results of those DID-ESR studies in three respects. First, the diffusion rates of the fluorescence-labeled sterol and phospholipid probes were nearly equal under all conditions of cholesterol concentration and temperature in the liquid crystalline state. Second, the temperature dependence of the self-diffusion coefficient was very mild in all compositions. Finally, self-diffusion coefficients of both fluorescence probes were almost constant until the concentration of cholesterol reached $x = 0.1$; they then decreased by factors of three at $x = 0.2$ but did not change much from $x = 0.2$ to 0.4. In all likelihood, the two experiments yielded different results because the photosensitive functional group attached to the parent molecules used in the FRAP experiments is very substantial in size and hence could have a dominant influence on the diffusional process. This could result in identical diffusion coefficients that are different from those of cholesterol and lipid.

Correlation Between Lateral Diffusion and Orientational Order Parameter

The most pronounced and important feature of the liquid crystalline phase is the existence of significant orientational order of the long axis of the phospholipid chains. This orientational order results from the mean ordering potential experienced by each molecule, which is usually taken to be that calculated in the mean field approximation, $U(\theta) = \rho(p,T)bS\,[(3\cos^2\theta - 1)/2]$, where θ is the angle between the long axis of the molecule and the direction of the average orientation (the director), S is the order parameter defined as $S = \int [(3\cos^2\theta - 1)/2] \exp[-U(\theta)/\mathcal{R}T]\, d(\cos\theta)$ while $\rho(p,T)$ is the number density, and b is the interaction constant. Figure 2 illustrates the results for S_{CSL} and $S_{16\text{-PC}}$ vs x for different temperatures in the binary POPC/cholesterol system. S_{CSL} increases sharply with x up to $x \approx 0.1$, but is not very

sensitive to further addition of cholesterol. The results for $S_{16\text{-PC}}$ show a more modest and gradual increase vs x. A comparison with Figure 1 shows that S and D have very similar but opposite trends vs x for both the labeled lipid and the labeled sterol. Equivalent observations were made for the DMPC-POPC-cholesterol system (70). As a result, an empirical relationship between D and S was established, and this relationship served as the basis for a model that explains how the structural changes in the membrane associated with the increased ordering from addition of cholesterol will influence the membrane fluidity as measured by D. Second, given that the nonlinear dependence of D_{CSL} on x and the very different behavior of $D_{16\text{-PC}}$ vs D_{CSL} with x are manifestations of nonideal solution behavior, the related behavior of S_{CSL} and $S_{16\text{-PC}}$ with x should also be attributed to nonideal behavior. In fact, for an ideal ordered fluid, S should vary linearly with composition (58).

We first consider the relationship between D and S. The empirical relation is of an Arrhenius form (68):

$$D(S,T) = D^0 \exp[-E(S,T)/\mathcal{R}T], \qquad 9.$$

where D^0 is the preexponential factor, $\mathcal{R}$ is the universal gas constant, and the activation energy $E(S,T)$ is given by:

$$E(S,T)/\mathcal{R} = \alpha(T)S^2(x,T) + \beta, \qquad 10.$$

with $\alpha(T)$ and β empirically determined. Figure 3 illustrates this relationship for both D_{CSL} and $D_{16\text{-PC}}$, in POPC-cholesterol mixtures. An equivalent result was found for DMPC-POPC-cholesterol mixtures (70). The values of $\alpha(T)$ and β appear in Table 1. What is most interesting about Equations 9 and 10 is that the only way the mole fraction of cholesterol, x, affects D is through the dependence of E on S. Finally, it is important to stress that the spectral measurements from which D and S were obtained were performed on the same sample during the same time period.

Correlation Between Rotational Diffusion and Orientational Order Parameter

The rotational diffusion tensor also reflects directly on the membrane fluidity. A very similar relationship to Equations 9 and 10 has been found for $R_{\perp,\text{CSL}}$, the perpendicular component of the rotational diffusion tensor for CSL (66, 68, 70), which measures the rate of reorientation of the long axis of CSL. In particular:

$$R_\perp = R_\perp^0 \exp[-AS^2(x,T)/\mathcal{R}T]. \qquad 11.$$

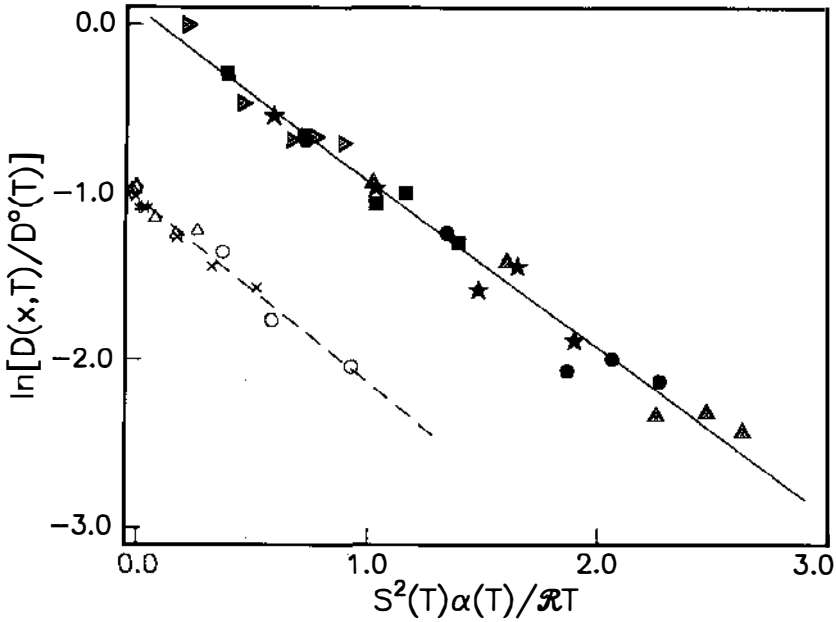

Figure 3 Plots of ln $D(x,T)$ − ln $D^0(T)$ vs $S^2(T)\alpha(T)/RT$ for CSL *(solid line)* and for 16-PC CSL *(dashed line)*, for the cholesterol mole fractions and temperatures shown in Figures 1 and 2. For 16-PC, ln $D(x,T)$ − ln $D^0(T)$ − 1 is plotted. Note $D^0(T) \equiv D^0 \exp(-\beta/RT)$. Data from Ref. 68.

Figure 4 displays an example of the validity of this relationship. (Here $A = 4.02$ kcal mol^{-1} and $R_\perp^0 = 2.02 \times 10^8$ s^{-1}.) Thus the overall rotational dynamics is also affected by the cholesterol simply through the structural change induced in the membrane, which is directly related to the order parameter. Similar comments also apply to the role of water (66), consistent with the fact that the cross-sectional area per lipid molecule is nearly proportional to the water content (43). Furthermore, if we recognize that the DID-ESR measurement of D is a macroscopic one ($\Delta x \approx 100$ μm and $t \approx 1$ h), whereas those of S and $R_\perp$ are microscopic ones (i.e. $\Delta x \approx$ molecular dimensions and $t \approx \tau_R \approx 3$–200 ns) such correlations imply temporal and spatial uniformity in the effects of mixing on dynamics characteristic of a single simple fluid solution.

No simple relation between $R_\perp$ and S emerged for labeled lipids 16-PC (68) and 7,6-PC (66). Unlike CSL, the lipid chain is nonrigid, so one must consider the complex internal modes of motion of the chain, as well as the overall molecular reorientation in any interpretation of $R_\perp$ (23).

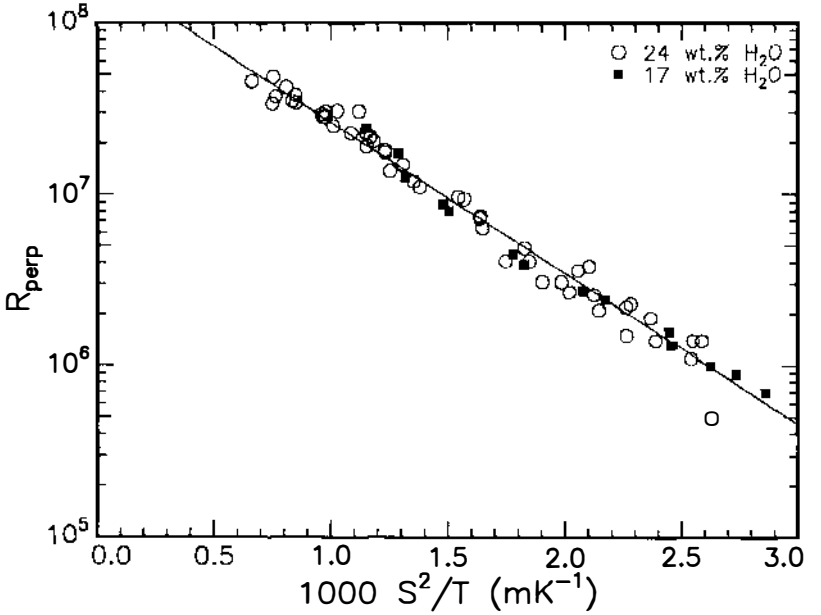

Figure 4 Semilog plot of $R_\perp$ for CSL vs S^2_{CSL}/T for a range of cholesterol mole fractions and temperatures in DMPC-cholesterol-H_2O mixtures. From Ref. 66.

FREE VOLUME MODEL

The S^2 dependence of the activation energy of lateral diffusion and of overall rotational reorientation can be interpreted within the context of the free volume model of Cohen & Turnbull (6). The principal concept of the free volume model is that each molecule of a system is confined to a cage by its neighbors. The molecule rattles inside this volume until fluctuations in density open a hole within the cage large enough to permit a substantial translation of the molecule.

If we introduce two characteristic free volumes, a critical free volume V^* that is large enough to permit a substantial displacement, and V^f, the average free volume per molecule, the diffusion coefficient can be expressed as (6): $D \approx D(V^*) \exp(-\lambda V^*/V^f)$, where $D(V^*)$ is the diffusion coefficient in a cage of volume $(V^* + \overline{V})$, $\overline{V}$ being the mean molecular volume. Because V^f can be assumed to arise from the isobaric thermal expansion, then

$$D = g(V^*)D^0(T) \exp[-\beta/(T - T_0)], \qquad 12.$$

where $\beta = \lambda\delta V/\alpha\overline{V}$, $\delta V = V^* - V^f$, α is the mean value of the thermal expansion coefficient, and T_0 is the temperature at which the volume

per molecule would be reduced to the close-packing limit. $D^0(T)$ is the small-scale diffusion constant, and $g(V^*)$ is a numerical factor related to the cage size for V^*, such that $D(V^*) = g(V^*)D^0(T)$. λ is a numerical constant. Usually $g(V^*)D^0(T)$ is written as $g^D \exp(-E_D/\Re T)$ where E_D is an activation energy associated with $D^0(T)$. Equation 12 explains the fluidity of numerous glass-forming substances (6). Vaz et al (74) applied it to PC model membranes, taking into account the drag forces at the membrane-water interfaces. Diogo & Martins (13) used an approach based upon the Cohen-Turnbull model to explain the twist viscosity in nematic liquid crystals, and Moscicki et al (48) used such a model to describe the translational diffusion in smectic liquid crystals. Also taking this approach, Shin et al (70) obtained a model explaining the composition and temperature dependence of lateral diffusion in mixed model membranes.

The ordering of the long molecular axis in membranes decreases the average free volume at the disposal of a molecule. Therefore, if the molecule is to gain the critical free volume, the cage must first expand by the amount that the orientational order has reduced it (ΔV^*), and second by the amount it would need in the fully disordered, or isotropic, fluid (i.e. δV). For phospholipid-cholesterol mixtures, one introduces the mean ordering potential experienced by a cholesterol molecule as: $U_{ch}(\theta) = -\rho_0[\xi b_{ch} S_{ch} + (1 - \xi) b_{lp} S_{lp}](3\cos^2\theta - 1)/2$, where ξ is the fractional average number of cholesterol molecules in the neighborhood of the CSL probe. Shin et al (70) show that for $T \gg T_0$ (cf Equation 11):

$$D_{ch}(T, S_{ch}) \approx g^D \exp\left(-\frac{E_D}{\Re T}\right) \times \exp\left[\frac{\beta_{or} + \xi\theta_{ch}S_{ch}^2 + (1 - \xi)\theta_{lp}S_{lp}S_{ch}}{T}\right], \quad 13.$$

where β_{or}, θ_{ch} and θ_{lp} are constants of the cholesterol (ch) and lipid (lp) mixture. Expressions for the diffusion coefficient of the phospholipid molecules can be written in the same fashion.

When the concentration of cholesterol is significant, cholesterol molecules experience mostly the cholesterol environment ($\xi \to 1$) according to the experimental results. Thus, $\xi\theta_{ch}S_{ch}^2 \to \theta_{ch}S_{ch}^2$ and $(1 - \xi)\theta_{lp}S_{lp}S_{ch} \to 0$ in Equation 13. This is just the form observed experimentally, implying that ξ approaches 1 at low mole fractions, x—i.e. the cholesterol molecules are aggregating. It would also appear that $\theta_{ch} \gg \theta_{lp}$. This result is consistent with the idea that for the elongated and structurally rigid cholesterol molecule, the intermolecular

interaction between cholesterol molecules is significantly larger than the interaction between the cholesterol probe and the phospholipid environment.

Shin et al (70) have shown that a very similar free volume approach may be applied to obtain an expression for $R_\perp$. For example, they obtain in the limit $\xi \rightarrow 1$, and $T \gg T_0$:

$$R_\perp(T,S_{ch}) \approx g^R_{ch} \exp\left(-\frac{E_R + \epsilon_{ch}S_{ch}}{\mathcal{R}T}\right) \exp\left(-\frac{\beta_{ch} + \theta_{ch}S^2_{ch}}{T}\right). \quad 14.$$

The definition of terms is essentially the same as for Equation 13 except that the β_{ch} and θ_{ch} in Equation 14 are of different magnitude than in Equation 13. A comparison of Equation 14 with experiment shows that $\theta_{ch}S^2_{ch}$ is the dominant term in the effective activation energy for $R_\perp$. The observations are consistent with a θ_{ch} for D_{CSL} being less than that for $R_{\perp CSL}$, implying a more crucial dependence of the rotational diffusion on the free volume.

THE ORDER PARAMETER AND THERMODYNAMICS

Given the important relationships between the diffusion coefficients and the order parameter, some further discussion of S is appropriate. S, an important thermodynamic quantity, results from the statistical average of the orienting forces (or torques) from the surrounding molecules. Thus, S for the ith component in a multicomponent system should reflect the average local composition of surrounding molecules. The ordering of the rigid CSL spin probe is particularly important in this context, because it has no intramolecular modes of motion, and it reports the overall ordering in the solution (36). For a label on a flexible chain position, one must correct the observed order parameter for the additional effects of internal motional averaging (23, 63).

The order parameter of the ith component and its activity in solution should be connected. We have explored this possibility (65, 66, 68, 69) and have proposed a general method for obtaining the activity coefficients of the components of mixed model membranes from the composition dependence of their orientational order parameters. The basic approach has been tested on phospholipid-cholesterol-water systems, partly in conjunction with the DID-ESR experiments. The order parameter for the ith component, S_i, is an intensive thermodynamic property somewhat analogous to the partial pressure (57, 69). Thus, S_i should be a linear function of the composition variable(s) if the solution

is ideal. When S_i varies nonlinearly with x_i (cf Figure 2), the replacement of x_i by the activity of the ith component should reestablish the linear nature of the functional dependence, just as it does other intensive thermodynamic properties of a solution. An analysis of the data on S_i for CSL and a labeled lipid (16-PC and 7,6-PC) vs cholesterol mole fraction showed that the activities obtained satisfied a necessary requirement of thermodynamics (i.e. the Gibbs-Duhem equation) (57).

Classical thermodynamics suggests that the most important thermodynamic quantity in the study of mixtures is the activity of each component. The activities of components in a binary mixture are related to each other by the Gibbs-Duhem equation. The variation of the activity (or equivalently the order parameter) of PC molecules can be predicted by integrating the Gibbs-Duhem equation once the activity of cholesterol is obtained. The good agreement of such predictions with the experimental results for PC-analog spin probes has three important implications: *(a)* the PC-cholesterol mixture forms a single phase solution, because the Gibbs-Duhem equation is only valid for components in single phase mixtures; *(b)* obtaining the thermodynamic activities from the order parameters is valid; and *(c)* one need only obtain the activity of one component as a function of all composition variables, because the activities of all other components can be calculated by integrating the Gibbs-Duhem equation (65, 66, 68, 69).

We also showed that the activities obtained from the order parameter can correctly predict the observed phase boundary between the single liquid crystalline phase for lower x_{ch} and the two-phase region for higher x_{ch}. Thermodynamic stability conditions for binary mixtures demonstrate that the chemical potential of a component should increase vs its mole fraction as long as the mixture is stable. However, the chemical potential, and hence the activity (or the order parameter), must reach its maximum at the phase boundary. Therefore, one can predict the phase boundary directly from the measured order parameter.

The obtained activities are consistent with the results of D_{CSL} and $D_{16\text{-PC}}$ in that they show nonideal mixing between lipid and cholesterol that leads to aggregation of cholesterol. They also showed that acyl chain unsaturation leads to poorer mixing of cholesterol in the PC model membranes (for $T > 35$°C) in the liquid crystalline phase. However, in a mixed solvent consisting of two types of lipid (DMPC and POPC), the dissolved cholesterol deviates less from ideality than it does in either of the two binary lipid–cholesterol mixtures.

Almost all the mixing properties may be deduced from the thermodynamic activities of the components. However, in the case of

mixed membranes a practical method has not been available for measuring the thermodynamic activities of the membrane components. Consequently, investigators could characterize the nonideal behavior of mixed membranes only indirectly, e.g. by comparing the phase diagram with that predicted using an appropriate theory (34, 35, 41). However, tractable theories are necessarily very approximate, and reliable data on thermodynamic activities in membranes would also enable one to accurately test and refine theoretical models. Feigenson (21) has developed a reliable experimental method based on solubility products. This method is, however, only applicable to systems containing phosphatidylserines. Thus a general method, such as that proposed by Shin & Freed, could be extremely valuable if it can be extended to a wide range of mixed membranes.

SPECTRAL-SPATIAL IMAGING: MACROSCOPIC VS MICROSCOPIC DIFFUSION

Spectral-spatial (SS) ESR imaging (19, 44, 45) is a promising technique for generalizing DID-ESR in order to study diffusion of spin probes in systems with substantial spin concentration. SS ESR imaging provides a way to resolve the concentration (or position)-dependent spectral variation in a two-dimensional fashion, as illustrated in Figure 5—i.e. along one axis (the spatial axis) it gives the spin concentration profile, whereas along the other axis it gives the ESR spectrum at that position (and spin concentration). This method had previously been illustrated for the investigation of transport in nonuniform media (71) and for studying O_2 distributions (76).

This technique was successfully applied to the simultaneous measurement of both the macroscopic and microscopic diffusion coefficients, D_{macro} and D_{micro}, respectively, of a spin-labeled phospholipid (16-PC) in oriented multilayers of POPC utilizing a substantial spin concentration (67) (larger than for DID-ESR). If the spin probe is initially concentrated in a small region of the sample, its distribution will tend over time to become homogeneous via translational diffusion. By measuring several SS images at different times, one can analyze the spread of the concentration profile as a function of time to obtain the macroscopic diffusion coefficient from the diffusion equation, by analogy with DID-ESR. In addition, such an experiment will be equivalent to the spectra obtained from many different homogeneous samples that must be prepared with different spin concentrations for conventional ESR studies of Heisenberg spin exchange (HE) (4, 50, 60). The ESR line broadening that results from spin relaxation induced by spin-spin

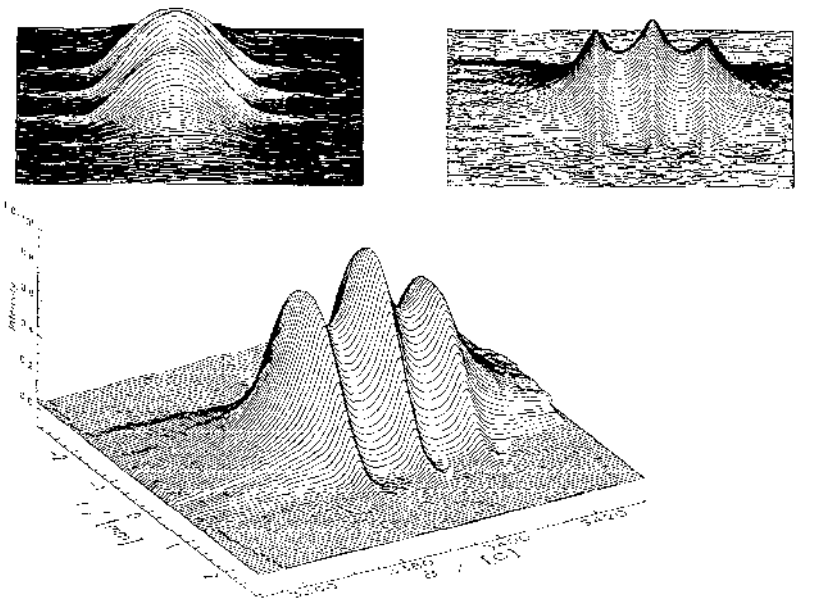

Figure 5 ESR spectral-spatial image of 16-PC diffusing in aligned multilayers of POPC viewed *(top left)* along the spectral axis to display the spatial distribution, *(top right)* along the spatial axis to display the spectral dependence on position, and *(bottom)* in perspective. From Ref. 67.

interactions such as HE can be analyzed to obtain the microscopic diffusion coefficient.

Devaux & McConnell (12) (prior to the development of ESR imaging) used the concentration dependence of the ESR spectra together with an inhomogeneous initial distribution of spin-labeled lipids to measure D_{macro}. The spatial distribution was deduced through a complicated simulation of the composite spectrum as a superposition of spectra from regions of different concentration. Spectral-spatial imaging effectively separates the spectra for each concentration, permitting a direct determination of D_{macro} from the time-dependent broadening of the concentration profile, as well as D_{micro} from the line broadening.

In comparing the results on macroscopic diffusion via ESR imaging vs microscopic diffusion via spin-spin interactions, one should remember that the former provides the macroscopic tracer diffusion coefficient of the spin label, which can be identified as the self-diffusion coefficient of the lipid when the two are very similar (68, 70). However, the latter provides a microscopic relative diffusion coefficient that is

very sensitive, not only to diffusion, but also to relative interactions between colliding spin labels, including how they are influenced by their milieu (14, 50). Also, any nonideal mixing of the spin labels will influence the probability of bimolecular collisions (14, 50).

The basic idea underlying SS imaging methods is that the spatial dependence of the ESR spectral intensity can be represented as a pseudo-object in a space consisting of an intrinsic frequency coordinate (the spectral dimension) and one or more spatial dimensions. The imaging method used is the multiple stepped gradient (19, 45) algorithm. In this technique, one sweeps through the ESR spectrum repeatedly, each time with a different constant magnetic field gradient. At each field gradient, $B'(\alpha)$, the spectrum obtained is the projection of the pseudo-object after it is rotated through some angle α, given by $B'(\alpha) = (\Delta I/\Delta x)\cot\alpha$ where ΔI is the spectral width and Δx is the size of the object. Once projections are collected for a set of rotation angles α, the image of the spectral-spatial object can be reconstructed using standard tomographic methods (19, 44, 77). In the diffusion experiment, the concentration distribution obtained by the multiple stepped gradient method was analyzed with Equation 6 for a Gaussian initial distribution given by Equation 8. The resultant Gaussian has a variance $\sigma^2(t) = \delta^2 + 2D_{\text{macro}}t$. Here t was 10 h, corresponding to an average molecular displacement, $\Delta x = (2Dt)^{1/2} \approx 400\ \mu$m and $D_{\text{macro}} = (2.3 \pm 0.4) \times 10^{-8}$ cm^2 s^{-1} at 22°C in agreement with the result from DID-ESR (68).

The concentration-dependent ESR line broadening arises from HE and from electron-electron dipolar (EED) interactions between the electron spins on neighboring spin probe molecules. According to modern HE theory (50), the Heisenberg spin exchange contribution to the line width, assuming isotropic three-dimensional Brownian diffusion, is given for ^{14}N nitroxides by

$$T_2^{-1}(\text{HE}) = (8\pi/3)\, dD_{\text{micro}} N_A C f^*, \qquad 15.$$

where d is the encounter distance for two spins, D_{micro} is the microscopic spin-label self-diffusion coefficient, N_A is the Avogadro number, C is the molar concentration of spins, and f^* is a partition function given by $(f^*)^{-1} = d\int_d^\infty \exp[U(r)/kT]r^{-2}\,dr$, in which $U(r)$ is a mean-field pair interaction potential for the spin probe molecules. By contrast, the EED contribution to the linewidth for isotropic motion is (50):

$$T_2^{-1}(\text{EED}) \approx \hbar^2\gamma_e^4 \left(\frac{19\pi}{405}\right)\left(\frac{N_A C}{dD_{\text{micro}}}\right)\left[\text{f}^* \exp\frac{U(d)}{kT}\right]^{-1} \qquad 16.$$

Equations 15 and 16 express the fact that the linewidth contributions from both HE and EED are linear with concentration in the limit of ideal solutions.

To make Equations 15 and 16 applicable to labeled lipids in membranes, the value of C was doubled to account for collisions between spin labels on different sides of the bilayer, following Sachse et al, because the nitroxide moiety is attached close to the end of one of the 16-PC acyl chains. These equations were also corrected for lateral (two-dimensional) diffusion in membranes by replacing the D_{micro} with $(2/3)D_{\text{micro}}$ (2, 50). With the assumption of Arrhenius behavior for D_{micro} [i.e. $D_{\text{micro}} = D^0 \exp(-E_{\text{act}}/kT)$], the temperature dependence of the concentration-dependent linewidth was used to separate T_2^{-1}(HE) and T_2^{-1}(EED). This separation leads to $E_{\text{act}} = 6.8 \pm 0.4$ kcal/mol, and $U(d) = 1.6 \pm 0.1$ kcal/mol. The result for E_{act} compares favorably with the value of $E_{\text{act}} = 6.3$ kcal/mol from D_{macro} measured for this system with DID-ESR (68). At 22°C, $D_{\perp,\text{micro}} = (1.0 \pm 0.4) \times 10^{-7}$ cm^2 s^{-1}. By comparison, linewidth studies by Sachse et al (60) yielded $D_{\text{micro}} \approx 1.2 \times 10^{-7}$ cm^2 s^{-1} (from the HE contribution) at 30°C for 16-PC in DMPC.

These measurements of D_{macro} and D_{micro} show that D_{micro} is about four times greater than D_{macro}. This result is in agreement with previous observations that D measured with microscopic techniques is larger than D measured with macroscopic techniques (39, 55). Pfeiffer et al (55) found that D_{micro} measured by quasielastic neutron scattering is approximately twofold larger than D_{macro} measured using FRAP in dipalmitoylphosphatidylcholine (DPPC) model membranes. Saxton (61) postulated that such discrepancies could result from different sample preparation techniques that produce inhomogeneous defects in the model membrane. However, the spectral-spatial measurements of D_{micro} and D_{macro} were carried out on the same sample.

The discrepancy between D_{macro} and D_{micro} may reflect important details in the microscopic molecular dynamics. Shin et al (67) point out that: *(a)* The d corresponding to the rigid diameter of the lipid may require correction for chain wagging (79). *(b)* The more subtle effects of two-dimensional motions in a plane and details of membrane structure may need to be included in the analysis of HE and EED (37, 80). The role played by nonideal mixing in the dynamic structure can also be important. Vaz & Almeida (73) have also considered discrepancies between D_{macro} and D_{micro} in the context of the free volume model.

In summary, the SS method provides an unambiguous comparison between D_{macro} and D_{micro} that eliminates possible artifacts resulting from differences in probe molecules, sample preparation, hydration,

etc, which are otherwise inevitable when D_{micro} and D_{macro} are measured using two different methods. We have suggested "such simultaneous measurements on various systems will provide an important tool to study the microscopic dynamic structure of membranes, and it will be extremely useful in the development of better models for molecular dynamics in membranes" (67, p. 955).

FOURIER TRANSFORM ESR IMAGING

Even though DID-ESR is now a well-developed technique, future developments are expected. For the most part, investigators have performed ESR imaging using cw methods. Researchers predominantly use the Fourier transform (FT) method in NMR imaging, but this method has been difficult to combine with ESR because of its higher frequencies, much shorter relaxation times, and much greater spectral bandwidths. FT-ESR imaging offers a number of advantages over cw methods, including faster data acquisition and more straightforward data analysis with fewer artifacts. A particulary nice feature of FT-ESR imaging applied to the DID-ESR experiment is that the Fourier-transformed spectra, $\hat{I}_g(\kappa,t)$ and $\hat{I}_0(\kappa)$ of Equations 2a and b are obtained directly by collecting the free induction decay (or else the echo decay). This permits one to obtain the Fourier-transformed concentration distribution $\hat{C}(\kappa,t)$ directly from the experiment, unlike in cw-DID-ESR where one must first Fourier transform $I_g(\xi,t)$ and $I_0(\xi)$ (17, 18, 47).

Spectral-spatial imaging, in particular, would benefit from FT imaging methods. FT imaging is much more flexible with respect to the possible combination of dimensions, both spectral and spatial, that can be presented in the final image. For example, one could perform two-(spectral) dimensional ESR in combination with one or more spatial dimensions. Thus modern two-dimensional Fourier transform (2D-FT)-ESR methods (28, 29, 53, 54) could enable ESR to measure molecular dynamics as a function of spatial coordinate.

Recent efforts in these laboratories have overcome the significant difficulties of FT-ESR imaging, and the method has been applied to spectral-spatial ESR imaging (17). In addition, we (18) have extended these techniques to spatially resolved two-dimensional electron-electron double resonance (2D-ELDOR). 2D-ELDOR is a form of two-dimensional exchange spectroscopy that is very sensitive to cross-relaxation processes such as HE (28, 29). Spatial resolution, would, for example, permit one to study microscopic molecular dynamics in inhomogeneous media. Most interesting is the potential application of

2D-ELDOR to the simultaneous study of both macroscopic and microscopic translational diffusion. This is likely to be an improvement over the cw method described above, in which the (inhomogeneously broadened) ESR linewidths are measured in the spectral dimension and the HE and EED are estimated from their concentration and temperature dependence to yield D_{micro} (30, 50). We have shown that 2D-ELDOR is a natural way to directly measure HE from the cross-peaks (28, 29). Thus, spatially resolved 2D-ELDOR could be the method of choice for comparative studies of microscopic vs macroscopic diffusion.

ACKNOWLEDGMENTS

I thank my coworkers, especially Drs. YK Shin and JK Moscicki for their considerable help and advice. This research was supported by NIH Grant GM25862 and NSF Grants CHE 9004552 and DMR 92-10638.

Literature Cited

1. Alecio MR, Golan DE, Veatch WR, Rando RR. 1982. Use of fluorescent cholesterol derivative to measure lateral mobility of cholesterol. *Proc. Natl. Acad. Sci. USA* 79:5171–74
2. Bales RL, Swenson JA, Schwartz RN. 1974. EPR studies of Heisenberg spin exchange in a nematic liquid crystal. *Mol. Cryst. Liq. Cryst.* 28:143–53
3. Berliner LJ, Fujii H. 1986. EPR imaging of diffusional processes in biologically relevant polymers. *J. Mag. Res.* 69:68–72
4. Berner B, Kivelson D. 1979. The electron spin resonance linewidth method for measuring diffusion. A critique. *J. Phys. Chem.* 83:1406–12
5. Cleary DA, Shin Y-K, Schneider DJ, Freed JH. 1988. Rapid determination of translational diffusion coefficients using ESR imaging. *J. Magn. Res.* 79: 474–92
6. Cohen MH, Turnbull D. 1959. Molecular transport in liquids and glasses. *J. Chem. Phys.* 31:1164–69
7. Crank J. 1976. *The Mathematics of Diffusion.* Oxford: The Clarendon
8. Crawford MS, Gerstein BC, Kuo, A-L, Wade CG. 1980. Diffusion in rigid bilayer membranes. Use of combined pulse and multiple pulse gradient techniques in nuclear magnetic resonance. *J. Am. Chem. Soc.* 102:3728–32
9. Demsar F, Cevc P, Schara M. 1986. Diffusion of spin probes in tissues measured by field-gradient EPR. *J. Mag. Res.* 69:258–63
10. Demsar F, Swartz HM, Schara M. 1988. Use of field gradient EPR to measure diffusion of nitroxides in tissues. *Mag. Res. Med. Biol.* 1:17–25
11. Demsar F, Walczak T, Morse PD II, Bacic G, Zolnai Z, et al. 1988. Detection of diffusion and distribution of oxygen by fast-scan EPR imaging. *J. Mag. Res.* 76:224–31
12. Devaux P, McConnell HM. 1972. Lateral diffusion in spin-labeled phosphatidylcholine multilayers. *J. Am. Chem. Soc.* 94:4475–81
13. Diogo AC, Martins AF. 1982. Order parameter and temperature dependence of the dynamic viscosity of nematic liquid crystals. *J. Phys.* 43:779–86
14. Eastman MP, Bruno GV, Freed JH.

1970. ESR studies of Heisenberg spin exchange II. Effects of radical charge and size. *J. Chem. Phys.* 52:2511–22
15. Eastman MP, Kooser RG, Das MR, Freed JH. 1969. Studies of Heisenberg spin exchange in ESR I. Linewidth and saturation effects. *J. Chem. Phys.* 51: 2690–2709
16. Eaton GR, Eaton SS, Ohno K, eds. 1991. *EPR Imaging and in Vivo EPR*. Boca Raton: CRC Press. 321 pp.
17. Ewert U, Crepeau RH, Dunnam CR, Xu D, Lee S, Freed JH. 1991. Fourier transform electron spin resonance imaging. *Chem. Phys. Lett.* 184:25–33
18. Ewert U, Crepeau RH, Lee S, Dunnam CR, Xu D, Freed JH. 1991. Spatially resolved two-dimensional Fourier transform ESR. *Chem. Phys. Lett.* 184:34–40
19. Ewert U, Herrling T. 1986. Spectrally resolved EPR tomography with stationary gradient. *Chem. Phys. Lett.* 129:516–20
20. Fahey PF, Koppel DE, Barker LS, Wolf DE, Elson EL, et al. 1976. Lateral diffusion in planar lipid bilayers. *Nature* 195:305–06
21. Feigenson GW. 1989. Calcium ion binding between lipid bilayers; the 4-component system of phosphatidylserine, phosphatidylcholine, calcium chloride, and water. *Biochemistry* 28: 1270–78
22. Feix JB, Yin JJ, Hyde JS. 1987. Interactions of ^{14}N; ^{15}N stearic acid spin-label pairs: effects of host lipid alkyl chain length and unsaturation. *Biochemistry* 26:3850–55
23. Ferrarini A, Nordio PL, Moro GJ, Crepeau RH, Freed JH. 1989. A theoretical model of phospholipid dynamics in membranes. *J. Chem. Phys.* 91: 5707–21
24. Freed JH. 1976. Theory of slow tumbling ESR spectra for nitroxides. In *Spin Labeling. Theory and Applications*, ed. LJ Berliner, pp. 53–132. New York: Academic
25. Galtseva EU, Yakimchenko YO, Lebedev YS. 1983. Diffusion of free radicals as studied by tomography. *Chem. Phys. Lett.* 99:301–4
26. Gennis RD. 1989. *Biomembranes, Molecular Structure and Function*. New York: Springer-Verlag. 533 pp.
27. Golan DE, Alecio MR, Veatch WR, Rando RR. 1984. Lateral mobility of phospholipid and cholesterol in the human erythrocyte membrane: effect of protein-lipid interactions. *Biochemistry* 23:332–39
28. Gorcester J, Freed JH. 1988. Two-dimensional Fourier transform ESR correlation spectroscopy. *J. Chem. Phys.* 88:4678–93
29. Gorcester J, Millhauser GL, Freed JH. 1990. Two-dimensional electron spin resonance. In *Modern Pulsed and Continuous-Wave ESR*, ed. L Kevan, MK Bowman, pp. 119–94. New York: Wiley
30. Gorcester J, Rananavare SB, Freed JH. 1989. Two-dimensional electron-electron double resonance and electron spin-echo study of solute dynamics in smectics. *J. Chem. Phys.* 90: 5764–86
31. Hawlicka E, Reimschuessel W. 1981. Component self-diffusion in liquid binary solutions. *Ber. Bunsenges. Phys. Chem.* 85:210–14
32. Hornak JP, Moscicki JM, Freed JH. 1984. *Translational diffusion coefficients by ESR imaging technique*. Presented at 7th Int. EPR Symp. Rocky Mountain Conference, Denver CO
33. Hornak JP, Moscicki JM, Schneider DJ, Freed JH. 1986. Diffusion coefficients in anisotropic fluids by ESR imaging of concentration profiles. *J. Chem. Phys.* 84:3387–95
34. Ipsen JH, Karlstrom GK, Mouritsen OE, Wennerstrom H, Zuckermann MJ. 1987. Phase equilibrium in the phosphatidylcholine-cholesterol system. *Biochim. Biophys. Acta* 905:162–72
35. Jan N, Lookman T, Pink DA. 1984. On computer simulation methods used to study models of two-component bilayers. *Biochemistry* 23:3227–32
36. Kar L, Ney-Igner E, Freed JH. 1985. ESR and electron-spin-echo studies of oriented multilayers of L_α-phosphatidylcholine water systems. *Biophys. J.* 48:569–93
37. Korb J, Ahadi PM, Zientara GP, Freed JH. 1987. Dynamic effects of pair correlation functions on spin relaxation by translational diffusion in two-dimensional fluids. *J. Chem. Phys.* 86: 1125–30
38. Krüger, GJ. 1982. Diffusion in thermotropic liquid crystals. Phys. Rep. 82:229–69
39. Kuo AL, Wade CG. 1979. Lipid lateral diffusion by pulsed nuclear magnetic resonance. *Biochemistry* 18:2300–8
40. Kusumi A, Subczynski WK, Pasenkiewicz-Gierula M, Hyde JH, Merkle H. 1986. Spin label studies on phosphatidylcholine-cholesterol membranes: effect of alkyl chain length and

unsaturation in the fluid phase. *Biochim. Biophys. Acta* 854:307–17
41. Lee AG. 1977. Lipid phase transitions and phase diagrams I. Lipid phase diagrams. *Biochim. Biophys. Acta* 472: 237–81
42. Lindbloom GL, Johansson BA, Arvidson G. 1981. Effect of cholesterol in membranes. Pulsed nuclear magnetic resonance measurements of lipid lateral diffusion. *Biochemistry* 20:2204–7
43. Lis LJ, McAlister M, Fuller N, Rand RP, Parsegian VA. 1982. Interactions between neutral phospholipid bilayer membranes. *Biophys. J.* 37:657–65
44. Maltempo MM, Eaton SS, Eaton GR. 1987. Spectral-spatial two-dimensional EPR imaging. *J. Magn. Reson.* 72:449–55
45. Maltempo MM, Eaton SS, Eaton GR. 1988. Reconstruction of spectral-spatial two-dimensional EPR images from incomplete sets of projections without prior knowledge of the component spectra. *J. Magn. Res.* 77:75–83
46. Moscicki JK, Shin YK, Freed JH. 1989. Dynamic imaging of diffusion by ESR. *J. Mag. Res.* 84:554–72
47. Moscicki JK, Shin YK, Freed JH. 1991. The method of dynamic imaging of diffusion by EPR. See Ref. 16, pp. 189–219
48. Moscicki JK, Shin YK, Freed JH. 1993. Translational diffusion in a smectic-a phase by ESR imaging: the free-volume model. *J. Chem. Phys.* 99:643–59
49. Mueller HJ, Galla HJ. 1987. Chain length and pressure dependence of lipid translational diffusion. *Eur. Biophys. J.* 14:485–91
50. Nayeem A, Rananavare SR, Sastry VSS, Freed JH. 1989. Heisenberg spin exchange and molecular diffusion in liquid crystals. *J. Chem. Phys.* 91: 6887–6905
51. Noack F. 1984. NMR studies of self-diffusion in some homologous nematic liquid crystals. *Mol. Cryst. Liq. Cryst.* 113:247–68
52. Pali T, Ebert B, Horvath LI. 1992. Dynamic imaging and spatially localized ESR spectroscopy of oriented phospholipid multilayers. *J. Magn. Res.* 96:491–500
53. Patyal BR, Crepeau RH, Gamliel D, Freed JH. 1990. Two-dimensional fourier transform ESR in the slow-motional and rigid limits: SECSY-ESR. *Chem. Phys. Lett.* 175:445–52
54. Patyal BR, Crepeau RH, Gamliel D, Freed JH. 1990. Two-dimensional fourier transform ESR in the slow-motional and rigid limits: 2D-ELDOR. *Chem. Phys. Lett.* 175:453–60
55. Pfeiffer WG, Schlossbauer G, Knoll W, Farago B, Steyer A, et al. 1988. Ultracold neutron scattering study of local lipid mobility in bilayer membranes. *J. Phys. France* 49:1077–82
56. Popp CA, Hyde JS. 1982. Electron-electron double resonance and saturation-recovery studies of nitroxide electron and nuclear spin-lattice relaxation times and Heisenberg exchange rates: lateral diffusion in dimyristoyl phosphatidylcholine. *Proc. Natl. Acad. Sci. USA* 79:2559–63
57. Prausnitz JM, Lichtenthaler RN, Azevido EG. 1986. *Molecular Thermodynamics of Fluid-Phase Equilibria*. Englewood Cliffs: Prentice-Hall. 2nd ed.
58. Rananavare SB, Pisipati VGKM, Freed JH. 1987. Nematic ordering near a tricritical nematic-smectic A phase transition. *Chem. Phys. Lett.* 140:255–62
59. Rubenstein JLR, Smith BA, McConnell HM. 1979. Lateral diffusion in binary mixtures of cholesterol and phosphatidylcholines. *Proc. Natl. Acad. Sci. USA* 76:15–18
60. Sachse J, King DM, Marsh D. 1987. ESR determination of lipid translational diffusion coefficients at low spin-label concentrations in biological membranes, using exchange broadening, exchange narrowing, and dipole-dipole interactions. *J. Magn. Res.* 71: 385–404
61. Saxton MJ. 1989. Lateral diffusion in an archipelago. Distance dependence of the diffusion coefficient. *Biophys. J.* 516:615–22
62. Schneider DJ, Freed JH. 1989. Calculating slow motional magnetic resonance spectra: a user's guide. In *Biological Magnetic Resonance*, ed. LJ Berliner, J Reuben, 8:1–76. New York: Plenum
63. Seelig J. 1977. Deuterium magnetic resonance; theory and application to lipid membranes. *Q. Rev. Biophys.* 10: 353–418
64. Shimshik EJ, McConnell HM. 1973. Lateral phase separation in phospholipid membranes. *Biochemistry* 12: 2351–60
65. Shin YK. 1990. *Thermodynamics and dynamics of phosphatidylcholine-cholesterol mixed model membranes: an*

ESR study. PhD thesis, Cornell Univ., Ithaca, NY. 170 pp.
66. Shin YK, Budil DE, Freed JH. 1993. Thermodynamics and dynamics of phosphatidylcholine-cholesterol mixed model membranes in the liquid crystalline state: effects of water. *Biophys. J.* 65:1283–94
67. Shin YK, Ewert U, Budil DE, Freed JH. 1991. Microscopic versus macroscopic diffusion in model membranes by ESR spectral-spatial imaging. *Biophys. J.* 59:950–57
68. Shin YK, Freed JH. 1989. Dynamic imaging of lateral diffusion by electron spin resonance and study of rotational dynamics in model membranes. Effect of cholesterol. *Biophys. J.* 55:537–50
69. Shin YK, Freed JH. 1989. Thermodynamics of phosphatidylcholine-cholesterol mixed model membranes in the liquid crystalline state studied by the orientational order parameter. *Biophys. J.* 56:1093–1100
70. Shin YK, Moscicki JK, Freed JH. 1990. Dynamics of phosphatidylcholine-cholesterol mixed model membranes in the liquid crystalline state. *Biophys. J.* 57:445–59
71. Stemp EDA, Eaton GR, Eaton SS, Maltempo MM. 1987. Spectral-spatial EPR imaging and transport of radicals in nonuniform media. *J. Phys. Chem.* 91:6467–69
72. Trauble H, Sackmann E. 1972. Phase transition of lipid model membranes. III. Structure of a steroid-lecithin system below and above the lipid-phase transition. *J. Am. Chem. Soc.* 94: 4499–4510
73. Vaz WLC, Almeida PF. 1991. Microscopic vs. macroscopic diffusion in one-component fluid phase lipid bilayer membranes. *Biophys. J.* 60: 1553–54
74. Vaz WLC, Clegg RM, Hallmann D. 1985. Translational diffusion of lipids in liquid crystalline phase phosphatidylcholine multilayers. A comparison of experiment with theory. *Biochemistry* 24:781–86
75. Wade CG. 1977. NMR relaxation in thermotropic liquid crystals. *Annu. Rev. Phys. Chem.* 28:47–73
76. Woods RK, Dobrucki JW, Glockner JF, Morse PD II, Swartz HM. 1989. Spectral-spatial ESR imaging as a method of noninvasive biological oximetry. *J. Magn. Reson.* 85:50–59
77. Woods RK, Hyslop WB, Marr RB, Lauterbur PC. 1991. Image reconstruction. See Ref 16, pp. 92–117
78. Wu ES, Jacobson K, Papahadjopoulous D. 1977. Lateral diffusion in phospholipid multilayers measured by fluorescence recovery after photobleaching. *Biochemistry* 16:3936–41
79. Yin JJ, Feix JB, Hyde JS. 1990. Mapping of collision frequencies for stearic acid spin labels by saturation-recovery EPR. *Biophys. J.* 58:713–20
80. Zientara GP, Freed JH. 1979. Chemically-induced dynamic spin polarization in two dimensional systems: theoretical predictions. *J. Chem. Phys.* 71: 3861–79